Microstructure and erosion characteristic of nodular cast iron surface modified by tungsten inert gas

Article *in* Materials and Design · March 2012

DOI: 10.1016/j.matdes.2011.09.029

CITATIONS
15

READS
48

1 author:

Jaafar Hadi Abboud
University of Babylon
34 PUBLICATIONS **663** CITATIONS

SEE PROFILE

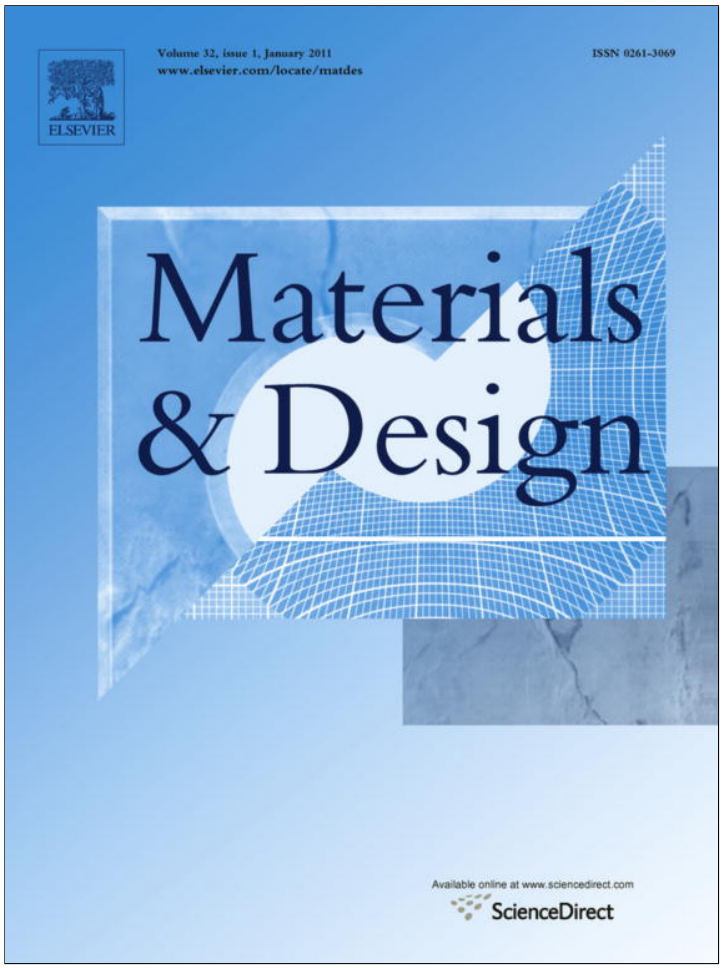

(This is a sample cover image for this issue. The actual cover is not yet available at this time.)

Materials and Design 35 (2012) 677–684

Contents lists available at SciVerse ScienceDirect

Materials and Design

journal homepage: www.elsevier.com/locate/matdes

Microstructure and erosion characteristic of nodular cast iron surface modified by tungsten inert gas

Jaafar Hadi Abboud *

Mechanical Engineering Department, Faculty of Engineering, University of Benghazi (Previously Garyounis), P.O. Box 1308, Benghazi, Libya

ARTICLE INFO

Article history:
Received 5 April 2011
Accepted 5 September 2011
Available online 15 October 2011

Keywords:
A. Nodular cast iron
C. Surface melting
F. Microstructure

ABSTRACT

The surface of nodular cast iron has been melted and rapidly solidified by Tungsten Inert Gas (TIG) process to produce a chilled structure of high hardness and better erosion resistance. Welding currents of magnitude 100, 150, and 200 A at a constant voltage of 72 have been used to melt the surface of nodular cast iron. Microstructural characterization, hardness measurements, and erosion wear tests have been performed on these modified surfaces as well as on the untreated material. Microstructural characterization has shown that surface melting resulted in complete or partial dissolution of the graphite nodules and resolidification of primary austenite dendrites, which undergo further decomposition into ferrite and cementite, and interdendritic of acicular eutectic; their microhardness measured across the melted depth ranged between 600 and 800 Hv. The scale of the dendrites and the interdendritic eutectic became coarser when a higher current is used. The results also indicated that remelting process by TIG improved erosion resistance by three to four times. Eroded surface observations of the as-received and TIG melted samples showed a ductile behavior with a maximum erosion rate at 30°. The fine microstructures obtained by the rapid cooling and the formation of a large amount of eutectic cementite instead of the graphite have contributed greatly to the plastic flow and consequently to the better erosion resistance of the TIG surface melted samples.

1. Introduction

Nodular cast irons, which are a relatively new addition to the cast iron family, became important engineering materials due to their high strength and toughness and relatively low price in addition to their excellent castability and machinability [1,2]. However, this material encounters severe erosion when it is used in many facilities such as air pressure pumps, gas delivery pipes and automatic sand molding equipment in casting industry. Many investigators, who studied the erosion resistance of nodular and gray cast irons in the as cast or after subsequent heat treating conditions, have point out the importance of graphite morphology and matrix structure in the erosion rates of the cast irons. Graphite phases seem to be detrimental to erosion resistance under a wide range of operating conditions [3–5]. Balan and his workers [4] have reported that the as cast gray cast iron exhibited the least resistance to erosion compare to the as cast nodular cast iron and heat treatment including quenching in oil from 880 °C and subsequent tempering for 1 h at a temperature of 700 °C did not improve the erosion resistance at normal impinging angle while the erosion resistance decreased with the heat treatment at oblique impact angle. The resistance of the gray cast irons to cavitation – erosion has been evaluated by Okada et al. [5]. The researchers concluded that free graphite acts as a surface notch and thus reduces the resistance to cavitation – erosion.

In recent years, high energy beams such electron beam [6–8], TIG [9–11], plasma [12,13] and lasers [14–18] have been used extensively to improve wear and erosion of all types of cast irons including the white cast iron by the remelting hardening process. In this technique, the cast iron surface is partially remelted and rapidly solidifies. The rapid cooling during solidification leads to the formation of large amount of eutectic cementite instead of the soft graphite and by this technique, the sliding wear and erosion resistance were improved significantly due to the hard surface developed and to the refinement of the structure.

Because of the high cost of operating the lasers and the need of vacuum in electron beam, attention was focused in using cheap, flexible and easy to operate TIG welding apparatus for surface melting treatments to all types of cast irons. Besides filler materials are not needed in this process.

The arc in TIG which was defined as "a sustained electrical discharge through a high-temperature conducting plasma produced sufficient thermal energy so as to be useful for the joining of metals by fusion and also for surface treatments. TIG provides some significant advantages which include selective hardening, minimum part

* Tel.: +218 925312410.
E-mail address: jhabboud@garyounis.edu

0261-3069/$ - see front matter © 2011 Published by Elsevier Ltd.
doi:10.1016/j.matdes.2011.09.029

distortion, controllable case depth, and no requirement for a quenchant. Kashani Bozorg and his workers have used TIG for surface modification of austempered ductile iron with and without chromium addition [11]. It has been shown that a significant improvement in hardness and wear resistance were obtained after TIG treatment. However, erosion resistance has not been evaluated.

In the literatures concerning surface hardening of cast iron by laser or electron beam remelting, there have been many studies on the sliding wear of nodular cast iron [19–21] but there is a little published work on erosion characteristics of TIG processed surface modified nodular cast iron.

The present work aims to use the TIG process as a heating source to modify the surface of the nodular cast iron by local remelting and hence improve hardness and erosion resistance and emphasizing on the modified structure from one side and to the erosion resistance at different impinging angles from the other side.

2. Experimental technique

2.1. Material

The material used in this research is nodular cast iron (NCI) taken from a 12.5 mm thick slice cut from a 0.5 m diameter tube. The slice was flattened and cut into many samples each one 15 mm wide and 60 mm long. The chemical composition is shown in Table 1, in which carbon content was 3.58 wt.% and Si around 2.4 wt.%. The surface of all pieces were ground and polished to a 5 μm finished and etched lightly to roughen the surface and decrease surface reflection. Fig. 1 is an optical micrograph of the NCI substrate, which consists of graphite nodules with average nodule diameter of 16 μm surrounded by ferrite and some pearlite; the volume fraction of the graphite, ferrite and pearlite as deduced from image analysis was 10%, 81% and 9% respectively. The average hardness was 85 measured on HRB scale.

2.2. Surface melting

Surface remelting was carried out by using TIG welding apparatus choosing three heats input conditions specified in term of applied current with the voltage constant at 72 V. These conditions were 100 A–72 V, 150 A–72 V, and 200 A–72 V. The welding speed was about 5 mm/s. Argon gas at a flow rate of 11 of L/min was used as shielding gas during melting process. The tungsten electrode was 2.4 mm in diameter and 150 mm long. The distance between tungsten electrode to specimen surface was kept at 3 mm. Tracks of 4 mm width were overlapped by 50% to make a treated surface area on each samples (Fig. 2). After TIG melting the overlapped tracks were cut into several samples each one has a 20 mm long and 15 mm wide. These cross sectioned samples were analyzed for microstructure and microhardness.

2.3. Microstructure and hardness analysis

After surface melting by TIG, the cross section samples were ground, polished, and etched with 3% nital. Optical microscopy and scanning electron microscopy were used to examine the microstructure and identify the phases before and after melting. The X-ray diffraction was carried out using a high resolution

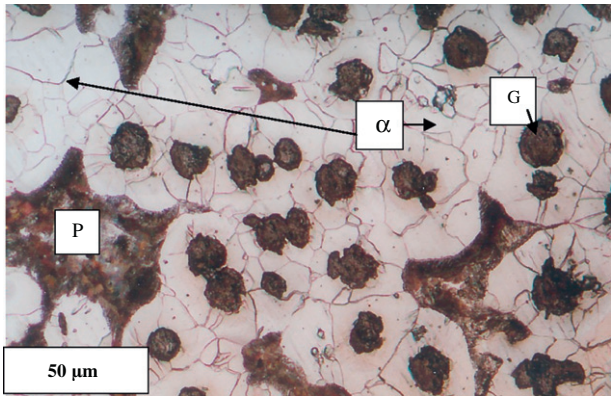

Fig. 1. Optical micrograph showing the microstructure of as-received NCI, α: ferrite, G: graphite and P: pearlite.

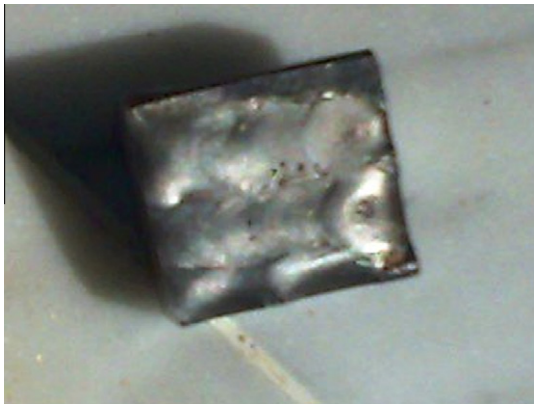

Fig. 2. Photograph showing three overlapped tracks produced on NCI substrate by TIG (200 A, 72 V).

Bruker Advance D8 XRD diffractometer in Bragg–Brentano geometry, with a Cu Kα monochromated beam (λ = 0.15406 Å) produced at 40 kV and 40 mA. The scanning electron microscope used in this experimental work was the 'EVO LS 15' developed by Carl Zeiss. Microhardness test using a load 200 g was performed on transverse sections across the depth.

2.4. Erosion test

For erosion test, three overlapped tracks covering a surface of 10 mm wide were produced at currents of 100 A, 150 A, and 200 A with a voltage of 72 V. The top surfaces were mechanically ground and polished with $800 > x > 300$ grit SiC paper to remove surface scales and obtain uniform and flat surface then subjected to erosion wear test at different angles. Both the as received and TIG melted surfaces were eroded in a typical sand blasted erosion apparatus shown in Fig. 3a–c. Angular Al_2O_3 particles of average size 500 μm were used as the erodent (Fig. 3a). Erodent particles were ejected by compressed air at a rate of about 35 g/s and at a speed of 30 m/s estimated by a double disks method [17] (Fig. 3b and c). The erosion stream is directed to impinge the sample surface at angles of 30°, 60°, and 90°, with constant distance between the

Table 1
Chemical composition of ductile cast iron.

Elements	Fe	%C	%Si	%Mn	%Mg	%Cr	%P	%S	%N
wt.%	Bal	3.58	2.4	0.2465	0.0235	0.0157	0.01	0.014	0.0278

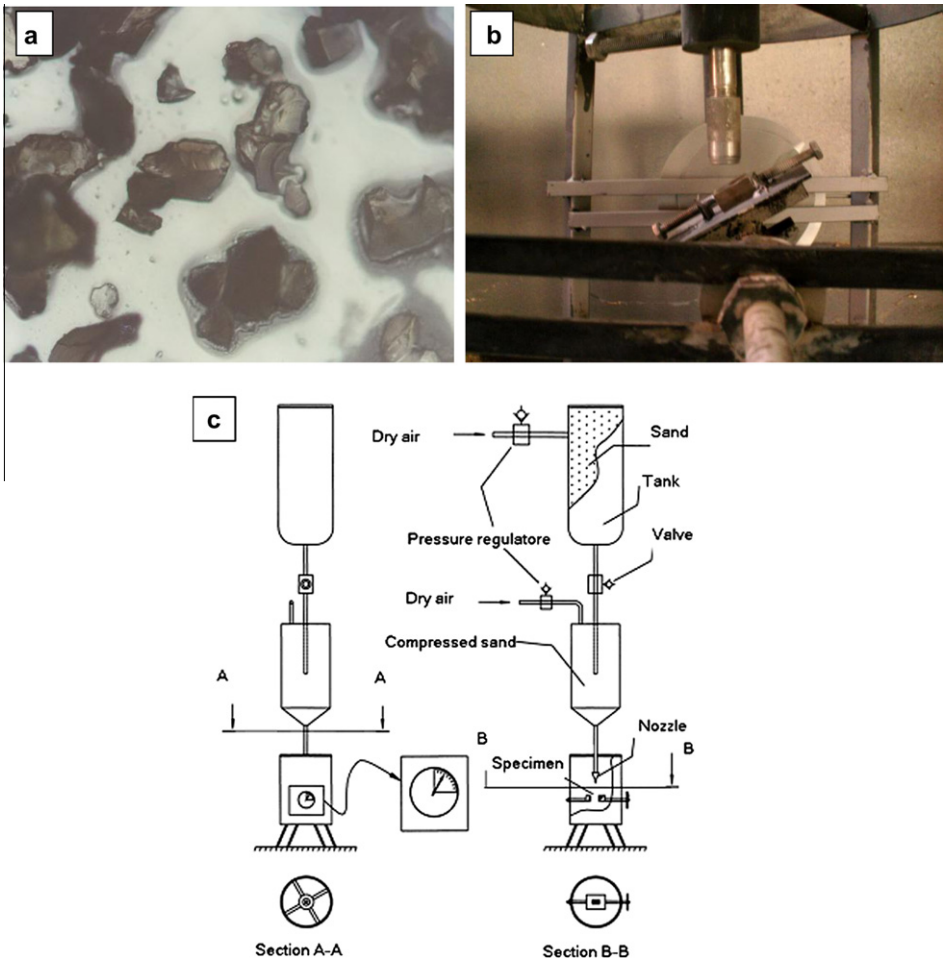

Fig. 3. (a) Al_2O_3 particles used in erosion test, (b) photograph shows the nozzle and the sample holder used in the erosion test, and (c) schematic diagram of the erosion test apparatus.

nozzle and sample set at 10 mm. The time period of each erosion test was 5 min, within which 2100 g Al_2O_3 particles were ejected. After completion of the erosion tests, the samples were cleaned with low pressure air and washed with alcohol. The weight loss caused by erosion was measured by microbalance of 0.01 mg accuracy. Initially, several untreated samples were tested at different condition to obtain steady state erosion and these parameters were fixed during the tests. Table 2 present the erosion conditions which are used in the present work.

3. Results and discussion

3.1. The microstructure

3.1.1. The melted zone (MZ)

During the TIG remelting process the cast iron surface was locally melted and rapidly solidified by self quenching. Due to rapid cooling effects, nucleation can be depressed to temperature well below the liquidus temperature and these undercooling results in the formation of a metastable Fe–Fe_3C phase instead of the equilibrium Fe-G system. Also, the microstructural features become refined because the time for coarsening during solidification is reduced. Fig. 4 shows cross sections of three treated layers produced at different currents. It is seen that the microstructure in all the melted layers contained primary dendrites accompanied by some light-etching fine Fe_3C crystals. The dendrites were aligned along specific directions. Some undissolve graphite nodules were also seen and their quantity increased with increasing current.

The depth of the melted layer increased with increasing current and a maximum value obtained was 2.5 mm using current 200 A (Table 3). No crack was observed in the melted zone or in the heat affected zone in all the processed layers. The macroscopic appearance comprising three distinctive zones namely the melted zone (MZ), irregular fusion interface (FI), and the heat affected zone (HAZ). There is an increase in the size of the melted depth and heat affected zone with increasing heat input (increasing current). The melted zone processed at 200 A showed a coarser structure with bigger dendrites as compared to the sample processed at 100 A which showed fine dendrites and eutectic of very fine spacing (see Fig. 4a and b). This result can be interpreted as due to a decrease of the cooling rate with increasing current. The melted zone produced at 200 A was bigger and cooled slower than the specimen processed at 100 A. From the other side it is shown that all the melted zones contain small amount of graphite nodules. The

Table 2
Erosion test conditions.

Specimen size (mm)	$15 \times 20 \times 12$
Abrasive	Al_2O_3 ($-800 + 300$ μm) of angular shape
Carrier gas	Dry air
Angle of impingement (°)	30, 60, and 90
Particle flow rate (g/s)	35
Particle velocity (m/s)	30
Test time (min)	5
Nozzle to specimen distance (mm)	10

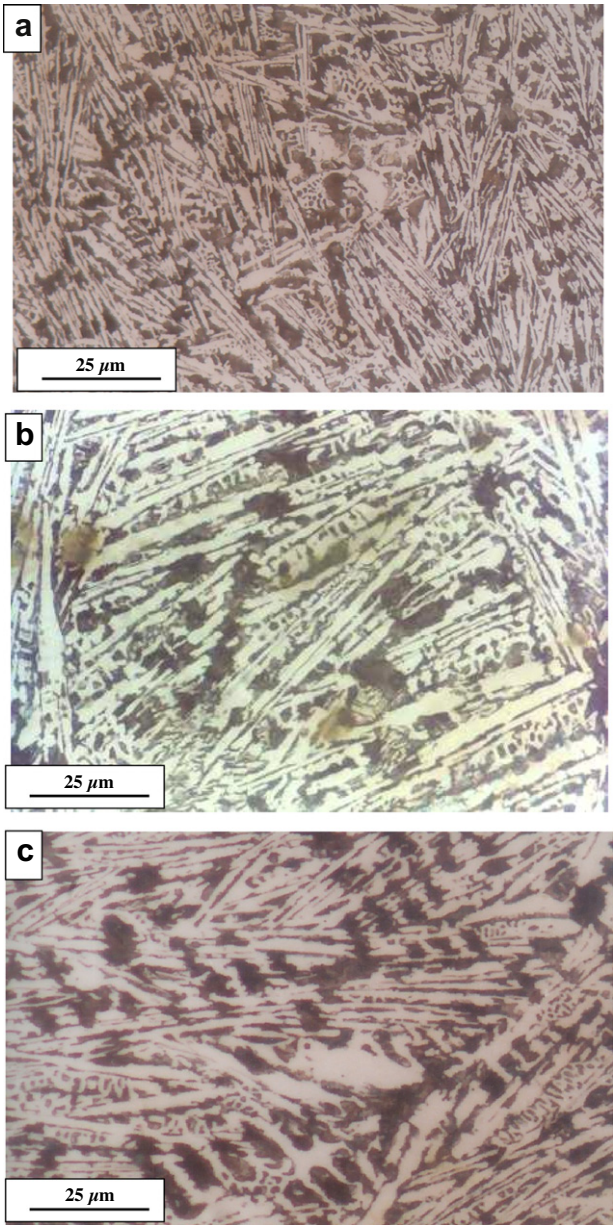

Fig. 4. Cross sectional microstructure showing the MZ produced by TIG at different currents: (a) 100 A, (b) 150 A, (c) 200 A, white areas-cementite; dark areas-transformed austenite.

Table 3
Effect of welding current on the melted zone depth, width, and average hardness.

Current (A)	Depth (mm)	Average hardness (HRC)
100	1.4	63
150	2.0	61
200	2.5	61

melted layer processed at 200 A showed more graphite than the sample processed at 100 A.

The microstructure taken by SEM of the melted zone processed at 100 A is shown with more detail in Fig. 5a–c. The eutectic structure is very fine and the cementite phase has a plate morphology with a thickness 1 μm and lengths more than 10 μm. The spacing between the eutectic plates is less than 0.5 μm. The eutectic grows sidewise as well as edgewise, resulting in a typical structure of white cast iron (see Fig. 5a). The

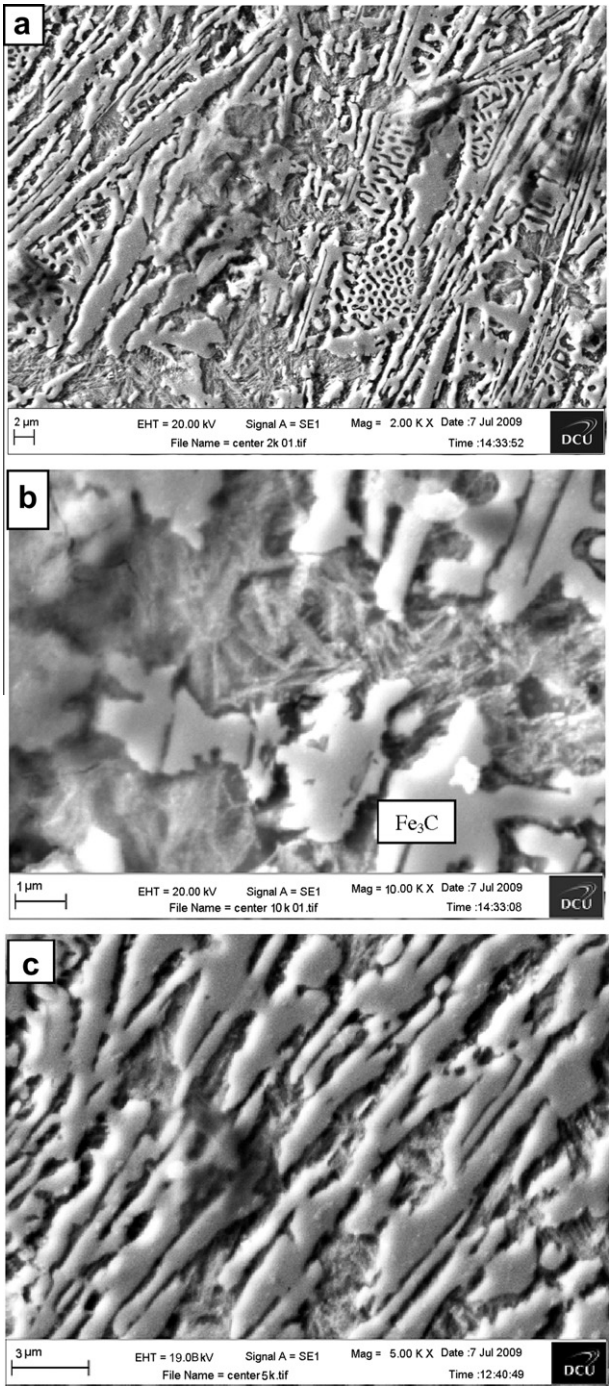

Fig. 5. (a–b) Scanning electron micrographs showing fine eutectic cementite, 100 A.

edgewise growth is more rapid than the sidewise mode and dominates the structure. These two shapes of cementite eutectic are due to different modes of growth of the quasi-regular structure. Hillert and Subba [22] have shown that once Fe_3C has nucleated, edgewise growth of Fe_3C plates occurs rapidly. They lead austenite at the interface and an orientation relationship develops (010) Fe_3C/(310) γ and (104) Fe_3C/(101)γ.

The dendritic structure has a preferred orientation inclined at an angle of 60° perpendicular to the solidification front. The dendrites accompanied by some light etching fine Fe_3C crystal and martensite (see Fig. 5b) and the region between the cementite eutectic display also a fine Fe_3C structure (see Fig. 5c).

X-ray diffractions performed on the surfaces of the as-received and surface melted layer at 100 A are shown in Fig. 6a and b. By comparing the *d* spacing or the position angles of the peaks with the standard peaks for ferrite, martensite, austenite, and cementite, it is clear that untreated cast iron showed alpha iron as the dominant phase while the melted surface layer showed strong peaks of cementite as well as peaks of ferrite α. No evidence of retained austenite was found. The broadening of peaks in the melted sample may be due to the strain accompanying the austenite to pearlite transformation as well as refinement of the microstructure, also the superposition of cementite peaks with ferrite. This result was consistent with the previous investigation carried out by TIG and electron beam [6–11].

3.1.2. The fusion line region

The irregular interface between the melted zone and the heat affected zone (HAZ) is the fusion line shown in Fig. 7. Rapid dissolution of the carbon from the graphite nodules into the surroundings occurs on the fusion line, resulting in a lowering of the melting point in that region. Melting occurs first in the close vicinity of the graphite nodules where the austenite matrix has been carbon enriched lowering the local melting point with a result of that the melt protrudes deeply into the neighboring zone. During solidification, fine and acicular eutectic comprised of thin and long cementite plates and transformed austenite are observed at the places adjacent to the graphite nodules.

3.1.3. The heat affected zone

At a small distance from the border line, partial dissolution of the graphite nodules was seen with the formation of eutectic cementite around the undissolved graphite. Coarse martensite plates are also seen between the undissolved graphite indicating austenization of the ferrite during the swift thermal cycle. However, due to the very short austenizing time, this martensite has low carbon and has a low hardness as found in this zone.

3.2. Microhardness

Although the hardness of the top melted layers was measured by HRC (see Table 2) with a maximum value ranging between 61 and 63 HRC, microhardness profiles across the melted depths from the surface for the three tracks processed at different currents were also performed and their results are shown in Fig. 8. It can be observed that the hardness of the melted zone increased sharply as

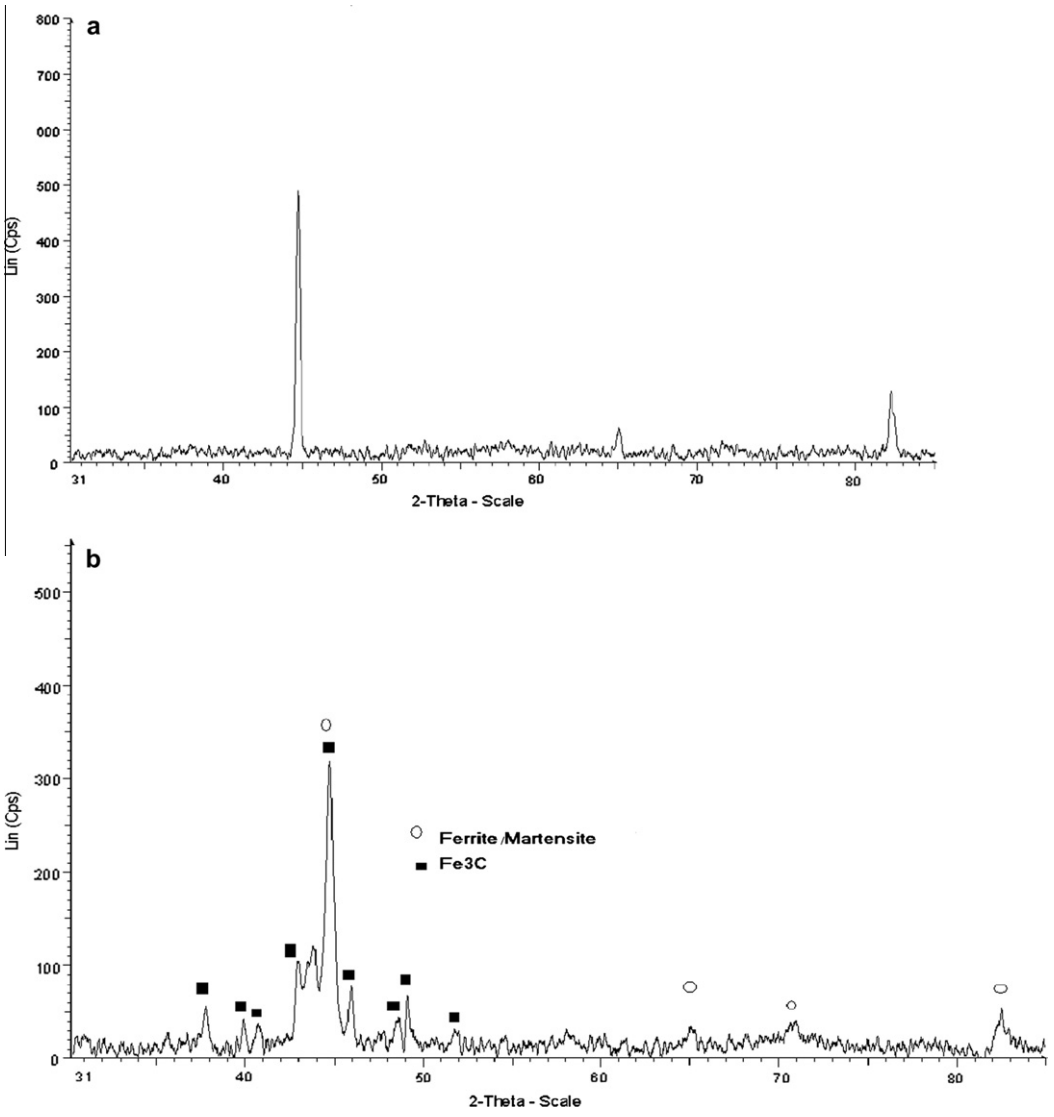

Fig. 6. (a) X-ray pattern of the as received NCI surface and (b) X-ray diffraction pattern taken from the TIG melted zone top surface (100 A, 72 V).

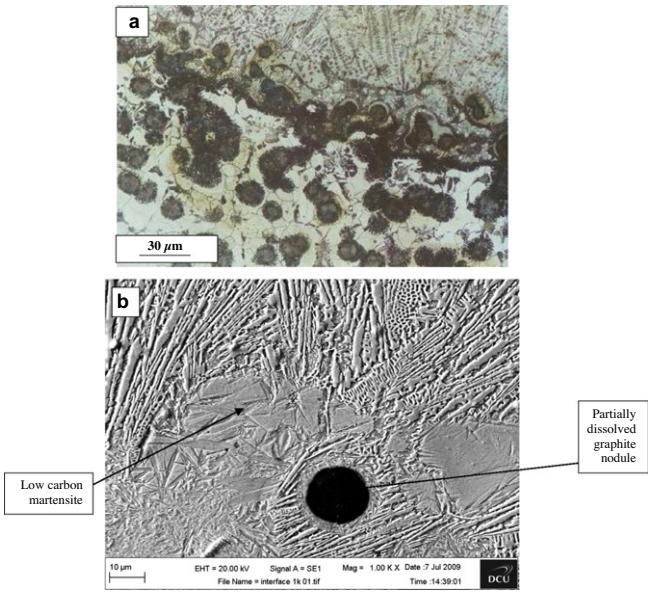

Fig. 7. (a) Optical micrograph showing the interface between the MZ and the HAZ and (b) SEM micrographs of the same region in (a).

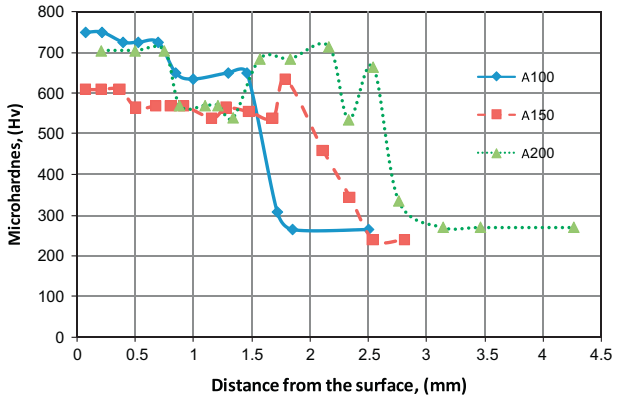

Fig. 8. Microhardness profiles across the melted depths of three surface layers obtained at a constant voltage and different currents.

compared to the hardness of as-received material. The melted zone processed at the lowest current 100 A showed a hardness level ranged between 650 and 750 Hv while at 200 A, it ranged between 550 and 700 Hv. It can be further observed that the hardness distribution across the melted depth is nearly uniform with a little fluctuation.

This significant increase in hardness can be attributed to the change of the microstructure from ferrite and graphite before melting to transformed austenite and cementite after melting by TIG. The melting and rapid solidification was enough to prevent graphite from nucleating in favor of cementite as shown by the micrographs. The cementite is very hard and the volume fraction of this phase increased after TIG melting. Also, from the microstructure analysis in Fig. 4 which showed more volume fraction of the acicular cementite with a very fine scale as compared to the sample processed at 200 A which showed a coarser dendrite and thick cementite plates compared to those processed at low current.

3.3. Erosion test

The variation of cumulative mass losses with blasting time for the as-received and TIG melted nodular cast iron samples eroded at 30° and 90° are shown in Fig. 9a and b, respectively. Generally, the cumulative weight loss increased linearly with blasting time. Furthermore, the erosion rates (which are measured from the slope of the curves) decreased significantly after TIG melting; the decrease in erosion rate is more pronounced in the sample processed at low current. Fig. 10 shows more clear the dependence of erosion on impact angles for the as-received and TIG melted samples. The results indicate that both the untreated and TIG melted have the highest erosion rates at the impact angle of 30° and the lowest rate at 90°. However, the curves (in Fig. 9a and b) show improvements in erosion resistance of about three to four times for the samples surface melted by TIG as compared with those untreated samples. The difference in the erosion rates versus angle is related to the mechanism of material removal in addition to the mechanical properties of the surfaces. It has been reported for a ductile material eroded at 90° that a huge part of the impact energy is spend on

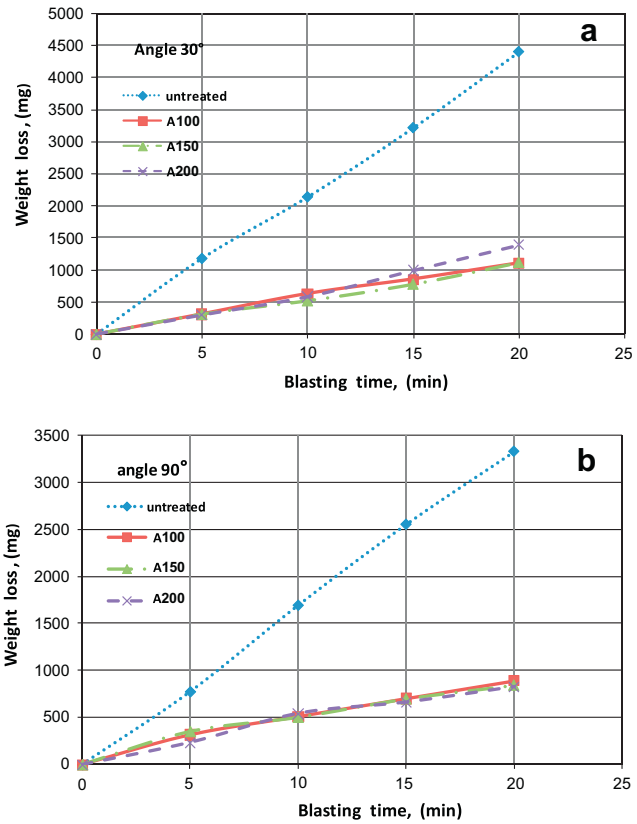

Fig. 9. Weight losses versus accumulated time for untreated and treated NCI at different impingement angles: (a) at 30° and (b) at 90°.

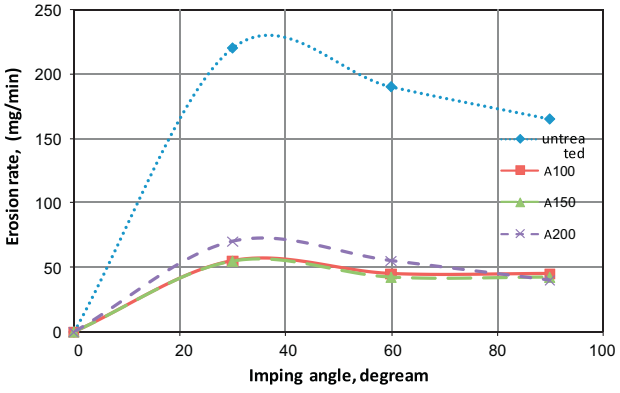

Fig. 10. Erosion rate versus impingement angles.

Table 4
Average erosion rates for as received and TIG melted samples.

Impinging angle	Erosion rate as received (mg/min)	Erosion rate, TIG melted		
		100 A (mg/min)	150 A (mg/min)	200 A (mg/min)
30	220	55	56	70
60	185	42	45	55
90	166	41	42	45

the formation of plastically deformed material on the surface and is absorbed by its high toughness. However, at a inclined impact angle, this deformed material is more readily removed as a result of the increase in the horizontal component of the impact energy.

The results of the present investigation indicate a typical ductile behavior of erosion for both untreated and TIG melted surfaces. Both demonstrate maximum erosion at inclined angle and minimum at normal angles. Table 4 presents the average erosion rate as a function of angle for both untreated and TIG processed samples. The data showed that low current is preferred and gives the lowest erosion rate. The improvements in erosion resistance after surface melting could be interpreted as due to the high hardness of the melted zone, finer structure, and formation of hard and tough eutectic containing large proportion of the hard cementite. Also, the elimination of the brittle graphite in favor of the hard cementite is another reason for this improvement in erosion resistance since it has been reported that the graphite nodules in cast irons seem to be detrimental to erosion resistance especially when it is formed in a soft matrix [19].

3.4. Mechanism of erosion

The material removal or displaced from the impacted surface can suffer several possible fates: it may be accommodated by elastic deformation of material away from the indentation, it may form a rim of plastically deformed material around the indentation, or it may be removed in some way by wear debris [3]. The possible mechanisms by which material can be removed depend on several factors such as the nature of the material wether it is ductile or brittle, the impact angle, and shape, size, and hardness of the erodent particles and their speed. Generally, for most ductile target materials and most types of erodent particles, the mass lost from the surface is closely proportional to the total mass of erodent particles which have struck the surface. The erosion of ductile materials depends strongly on impact angle showing a maximum at 20° or 30° [3]. For ductile materials, it has been reported that at normal angle, deformation is caused mainly by plastic deformation while at inclined angle; the deformation is caused by cutting. Several modes of cutting have been reported such as ploughing, chipping and cutting [3]. Strain hardening plays a significant role in material removal. Fig. 11 shows photographs of the top view of the eroded surfaces of untreated cast iron subjected to erosion tests at different angles. The as-received surface eroded at 90° showed a big crater of a circular shape with maximum depth 3.5 mm while the sample eroded at an inclined angle of 30° showed a bigger crater of elliptical shape. The TIG melted samples processed at different currents and tested with an impact angle of 90° showed a smaller crater with shallow depths of less than 1 mm. At 100 A current, the crater is very shallow (see Fig. 11, the first row sample). However,

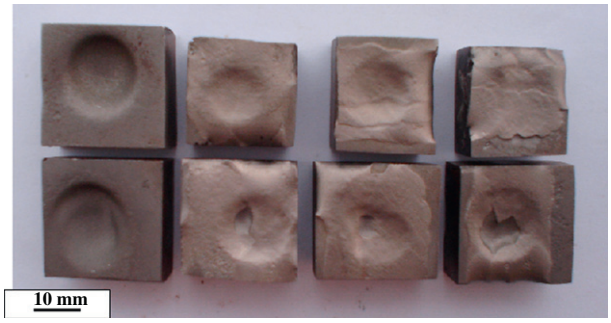

Fig. 11. Photograph showing the worn surface of the as received and TIG melted. From the left, the top samples are the as received and TIG melted samples at current 200 A, 150 A, and 100 A, respectively eroded at 90° and the lower are the as received and TIG melted samples (200 A, 150 A, and 100 A) eroded at 30°.

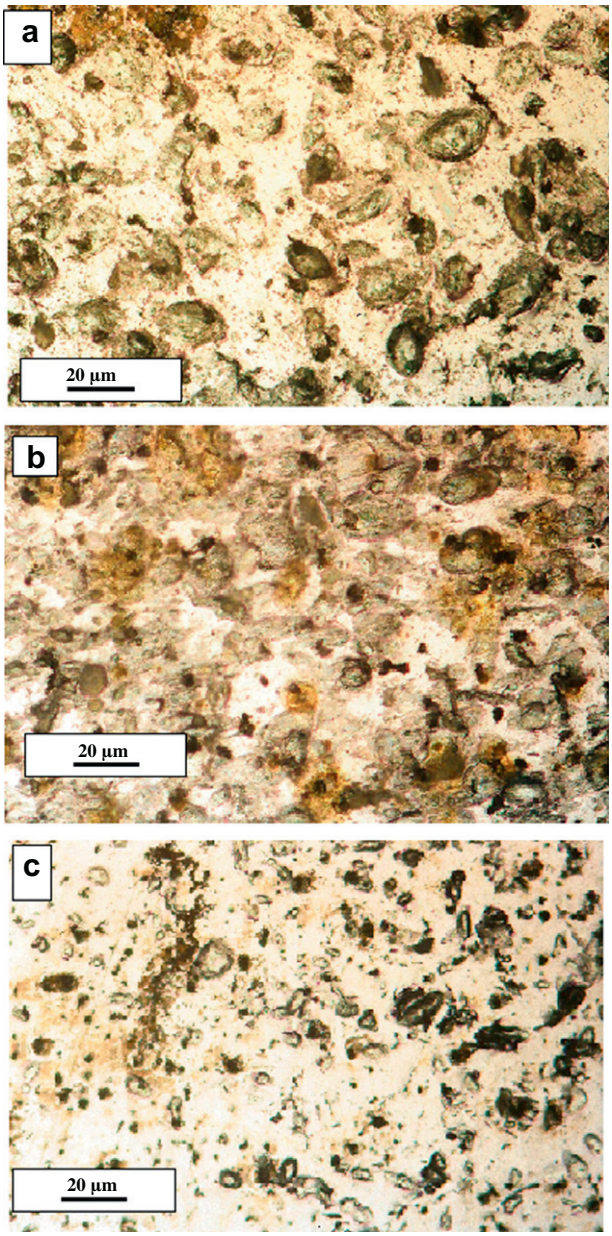

Fig. 12. Optical macrograph show the eroded surface on untreated nodular cast iron impinged at (a) 30°, (b) 60° and (c) 90°.

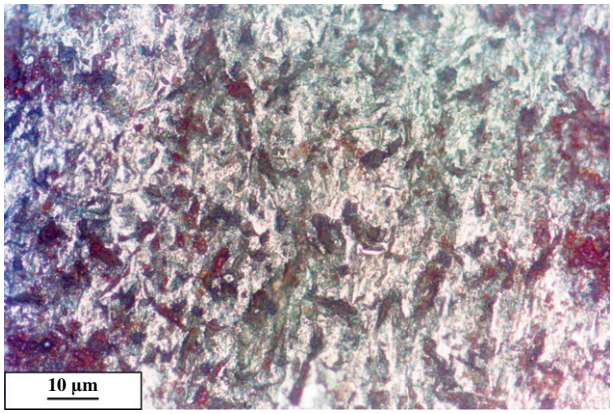

Fig. 13. Optical macrographs showing eroded surface of the melted layers impinged at an angle of 30°.

at 30°, the crater is relatively big and penetrated the substrate (Fig. 11, the second row samples). Generally, as in the as-received samples, the eroded area became bigger as the erosion angle decreased. The maximum penetration depth measured for the TIG melted sample eroded at 30° for 20 min blasting (42 kg erodent mass) was less than 1 mm which is much less than the as-received nodular cast iron which was ~3.5 mm. This indicates a greater resistance to plastic flow caused by the repeated impact of the erodent particles. Since the remelted zone has a higher hardness, more homogenous and fine structure, hence it is more flow-resistant.

In the present work effort has been made to examine the eroded surface by optical microscopy and also by mean of scanning electron microscopy. However because of uneven topography of the eroded surface at 20 min blasting, it was not possible to obtain significant information which may lead to knowledge of the mechanism of erosion. However, short-term erosion test of untreated NCI samples (erosion at few seconds) showed the presence of big and elongated scares in the samples eroded at 30°; while the scare is small with a circular shape in the sample eroded at 90° (Fig. 12a–c). These features give evidence of a ductile behavior of the untreated nodular cast iron. During erosion lip formation is apparent in these figures. The surface topography of the treated samples show similar features, but at a smaller scale (Fig. 13). The low erosion rate for the TIG melted sample particularly at 90° suggests that it is the resistance to plastic flow which governs the material removal rate (see Fig. 13).

4. Conclusions

Based on investigations of the microstructure and erosion properties of NCI surface melted by TIG, the following conclusions can be summarized:

(1) Local surface melting of NCI by TIG arc operated at currents of 100, 150 and 200 A and voltage 70–72 V resulted in the complete or partial dissolution of graphite nodules and resolidification of a dendrites of austenite accompanied by some light etching fine Fe_3C and intedendritic region of eutectic ledeburite.
(2) The microhardness of the treated layers is increased to a level ranged between 600 and 800 Hv. Increasing the current affected the scale of the microstructure and increased the hardening depth and the heat affected zone depth. However, the hardness level of the sample processed at 100 A current is higher than those treated at 150 and 200 A.
(3) The heat affected zone adjacent to the melted region, consists of plate martensite and partially dissolved graphite surrounded by eutectic structure.
(4) The experimental results of erosion test showed a significant improvement in erosion resistance after melting treatment by a factor of about 300%.
(5) A ductile behavior mode was found in both the as-received and TIG melted layer with a maximum erosion rate at 30° impinging angle.
(6) Remelting of the nodular cast iron by TIG without using filler material is a simple and a cheap way for producing hard surfaces with a unique microstructure and a high wear resistance.

Acknowledgment

The author expresses deep thanks to the Mechanical Engineering Department at Benghazi University for permitting to use the compressor for conducting the erosion test and to Dr. Khaled Benyounis in Dublin City University for his help in SEM.

References

[1] Angus HT. Cast iron – physical and engineering properties, 2nd ed. London: Butterworth and Co.; 1976 [chapter 1].
[2] Elliott Roy. Cast iron technology. London: Butterworth and Co.; 1988.
[3] Finnie Iain. Some reflections on the past and future of erosion. Wear 1995;1:186–7.
[4] Balan KP, Reddy AV, Joshi V, Sundararajan G. The influence of microstructure on the erosion behaviour of cast irons. Wear 1991;145:283–96.
[5] Okada T, Iwai Y, Yamamoto A. A study of cavitation erosion of cast iron. Wear 1983;84:297–312.
[6] Heydarzadeh MS, Karshenas G, Boutorabi SM. Electron beam surface melting of as cast and austempered ductile irons. J Mater Process Technol 2004;153–154:199–202.
[7] Jean M, Tzeng Y. Optimization of electron-beam surface hardening of cast iron for high wear resistance using the Taguchi method. Int J Adv Manuf Technol 2004;24:190–8.
[8] Gulzar A, Akhter JI, Ahmad M, Ali G, Mahmood M, Ajmal M. Microstructure evolution during surface alloying of ductile iron and austempered ductile iron by electron beam melting. Appl Surf Sci 2009;255:8527–32.
[9] Hiraoka T, Nakamora Y, Tanaka Y. Mechanical properties of cast iron surface-hardened by TIG arc remelting. Trans Am Foundrymen's Soc 1995(102):603.
[10] Amirsadeghi A, Heydarzadeh MS. Comparison of the influence of molybdenum and chromium TIG surface alloying on the microstructure, hardness and wear resistance of ADI. J Mater Process Technol 2008;201:673–7.
[11] Amirsadeghi A, Heydarzadeh MS, Kashani Bozorg SF. Effects of TIG surface melting and chromium surface alloying on microstructure, hardness and wear resistance of ADI. J Iron Steel Res Int 2008;15:86–94.
[12] Ishida T. Local melting of nodular cast iron by plasma arc. J Mater Sci 1983;18:1773–84.
[13] Dai WS, Chen LH, Lui TS. SiO_2 particle erosion of spheroidal graphite cast iron after surface remelting by the plasma transferred arc process. Wear 2001;248:201–10.
[14] Benyounis KY, Fakron OM, Abboud JH. Rapid solidification of M2 high-speed steel by laser melting. Mater Des 2009;30:674–8.
[15] Benyounis KY, Fakron OMA, Abboud JH, Olabi AG, Hashmi MJS. Surface melting of nodular cast iron by Nd-YAG laser and TIG. J Mater Process Technol 2005;170:127–32.
[16] Roy A, Manna I. Laser surface engineering to improve wear resistance of austempered ductile iron. Mater Sci Eng A 2001;279:85–93.
[17] Alabeedi KF, Abboud JH, Benyounis KY. Microstructure and erosion resistance enhancement of nodular cast iron by laser melting. Wear 2009;266:925–33.
[18] Chen CH, Ju CP, Rigsbee JM. Laser surface modification of ductile cast iron. Mater Sci Technol 1988;4:161.
[19] Chang LC, Hsui IC, Chen LH, Lui TS. Influence of graphite nodules on the particles erosion of spheroidal graphite cast iron. Wear 2004;257:1125–32.
[20] Arabi Jeshvaghani R, Shamanian M, Jaberzadeh M. Enhancement of wear resistance of ductile iron surface alloyed by stellite 6. Mater Des 2011;32:2028–33.
[21] Shamanian M, Mousavi Abarghouie SMR, Mousavi Pour SR. Effects of surface alloying on microstructure and wear behavior of ductile iron. Mater Des 2010;31:2760–6.
[22] Hillert M, Subba VV. Grey and white solidification of cast iron. Proc Solidific Metals 1986;204:110.